Chemical Engineering Journal 153 (2009) 211–216

Contents lists available at ScienceDirect

Chemical Engineering Journal

journal homepage: www.elsevier.com/locate/cej

# Direct synthesis of carbon and nitrogen–carbon nanospheres from aromatic hydrocarbons

Antonio Nieto-Márquez[a,*], Inmaculada Espartero[a], José Carlos Lazo[b], Amaya Romero[a], José Luis Valverde[a]

[a] Facultad de Ciencias Químicas, Departamento de Ingeniería Química, Universidad de Castilla-La Mancha, Campus Universitario s/n, 13071 Ciudad Real, Spain
[b] Sección Química, Departamento de Ciencias, Pontificia Universidad Católica del Perú, Av. Universitaria 1801, Lima 32, Peru

ARTICLE INFO

*Article history:*
Received 9 April 2009
Received in revised form 2 June 2009
Accepted 5 June 2009

*Keywords:*
Benzene
Aniline
Nitrobenzene
Pyrolysis
Carbon nanospheres

ABSTRACT

In the present work, a controlled production of carbon nanospheres (CNS) via pyrolysis of benzene, aniline and nitrobenzene at 950 °C has been examined. The nature of the carbonaceous product has been characterized by transmission electron microscopy (TEM), $N_2$ adsorption/desorption, X-ray diffraction (XRD), elemental analysis (CHN), temperature-programmed oxidation (TPO) and X-ray photoelectron spectroscopy (XPS). Time-on-stream served to enhance the spherical morphology of the product, as well as its crystalline character. Nitrogen inclusion resulted in an enhanced curvature of the graphene layers, as well as the incorporation of lattice defects, resulting in a less crystalline material. The reactive nature of the feed influenced the amount of nitrogen incorporated into the carbon matrix, as well as the kind and distribution of nitrogen functionalities.



## 1. Introduction

The discovery of nanostructured carbon materials has led to a big effort in their synthesis, preparation/purification and surface chemistry modification, given their promising applications in nanoelectronic devices, hydrogen storage or catalyst supports [1–3] among others. Arc discharge and laser ablation have been employed in the synthesis of structured carbon [4,5] but these methods also produce a significant quantity of undesired by-products, such as carbon soot, that necessitates additional purification steps. Moreover, the associated low yields and high energy requirements have served as the impetus for the development of more efficient carbon production processes. In this line, a termed chemical vapour decomposition (CVD) route (often in the presence of a catalyst), has emerged as a lower cost option which exhibits a greater degree of control and a more feasible scale-up [6]. Doping these carbonaceous structures with heteroatoms, such as nitrogen or boron, is an effective means of modifying surface and electronic properties [7,8]. Indeed, it has been established that the incorporation of nitrogen in nanotubes results in enhanced conductivity, polarity and basicity, while modifying surface hydrophilicity [9], as nitrogen can be considered an "n-type" dopant with an extra electron for donation when replacing carbon in the graphitic matrix. Carbon nanotubes (CNT) and carbon nanofibres (CNF) have attracted an enormous research interest in the last decade, with an exponential increase in the related literature. However, a targeted production of carbon nanospheres (CNS) is only now starting to achieve a significant research activity. Their high surface chemical activity provided by the unclosed graphitic layers, which provides reactive "dangling bonds" [10], makes them suitable materials for catalysis and adsorption processes. Moreover, CNS have also encountered application as lubricants, polymer additives, in energy storage and as precursors for diamond film synthesis [11]. Although the presence of carbon spheres in commercial carbon blacks is widely known, novel and selective production routes have been recently reported in the literature, such as the Li and K promoted reduction of $CO_2$ under supercritical conditions [12] and the Mg promoted reduction of methanol [13]. Several works report the growth of CNS by a catalyst assisted chemical deposition route; Kang and Wang reported the catalytic synthesis of CNS *via* the mixed-valent oxide decomposition of natural gas at 1100 °C [10,14,15]. Serp et al. reported the decomposition of $CH_4$, $C_5H_{12}$ and $C_2H_2$ over a range of Ni and Fe catalysts [11], but still conducted at elevated temperatures (700–1100 °C). In previous works, we reported the growth of CNS from the decomposition of $C_2HCl_3$ over $Ni/SiO_2$ at 600 °C [16,17]. Direct pyrolysis (CVD in the absence of a catalyst) of hydrocarbons has been reported as an effective means of producing CNS; Qian et al. obtained CNS from toluene at temperatures greater than 1000 °C [18] and Jin et al. reported the direct synthesis of carbon spheres from the pyrolysis of a range of hydrocarbons, including styrene,

* Corresponding author. Tel.: +34 926295300; fax: +34 926295256.
*E-mail address:* antonio.nieto@uclm.es (A. Nieto-Márquez).

1385-8947/$ – see front matter © 2009 Elsevier B.V. All rights reserved.
doi:10.1016/j.cej.2009.06.010

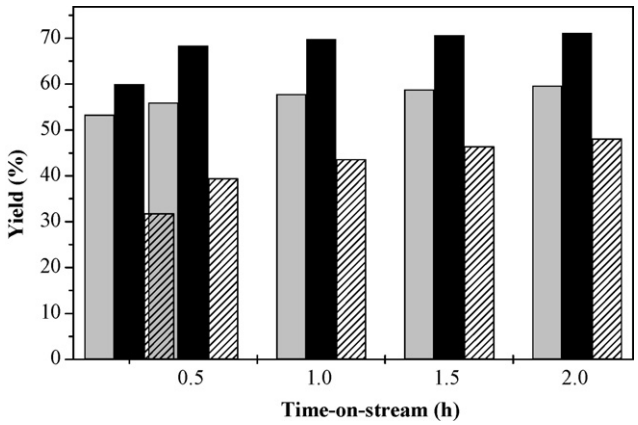


**Fig. 1.** Carbon yield as a function of time-on-stream for the pyrolysis of benzene (grey bars), aniline (black bars) and nitrobenzene (hatched bars).

toluene, benzene, hexane, cyclohexane and ethane in the temperature range 800–1200 °C [19]. It is also worth flagging the work of Yang et al., who produced CNS from the pyrolysis of polyacrylonitrile (PAN) [20]. To the best of authors' knowledge, no direct synthesis (in the absence of catalyst and/or template) of nitrogen-doped nanospheres has been reported before. In this line, we report a controlled growth of uniformly sized nanospheres from the direct pyrolysis of benzene, aniline and nitrobenzene. Physicochemical properties and nitrogen incorporation in the carbonaceous structures are discussed.

## 2. Experimental

### 2.1. Growth of carbon nanospheres

Carbon growth was carried out at atmospheric pressure and 950 °C in a continuous plug flow reactor (quartz tube, 3 cm i.d. × 60 cm) mounted in a temperature programmable oven. The aromatic feed was supplied by a Bronkhorst CEM (Controller Evaporator Mixer), using He as inert carrier gas. The ratio between aromatic precursor and He was maintained in all the cases at 1:4 (v/v), with a total inlet flow of 150 ml $min^{-1}$. Carbon growth was monitored for up to 2 h-on-stream. After each run, the reactor was cooled to room temperature in a flow of He prior to off-line analyses.

### 2.2. Carbon characterization

Powder X-ray diffractograms (XRD) were recorded with a Philips PW 1710 instrument using Ni-filtered Cu Kα radiation. Surface area/porosity measurements were conducted using a Micromeritics ASAP 2010 sorptometer apparatus with $N_2$ as sorbate at 77 K. Samples were outgased (at $5 \times 10^{-3}$ Torr) at 180 °C overnight prior to analysis. Specific total surface areas were calculated using the multi-point BET method and specific total pore volumes were evaluated from $N_2$ uptake at a relative pressure ($P/P_0$) = 0.99. Pore size distributions were evaluated using the standard Barrett–Joiner–Halenda (BJH) treatment. Carbon morphology/dimensions were analyzed by transmission electron microscopy (TEM), using a JEOL JEM-4000EX. Suitable specimens for TEM analyses were prepared by ultrasonic dispersion

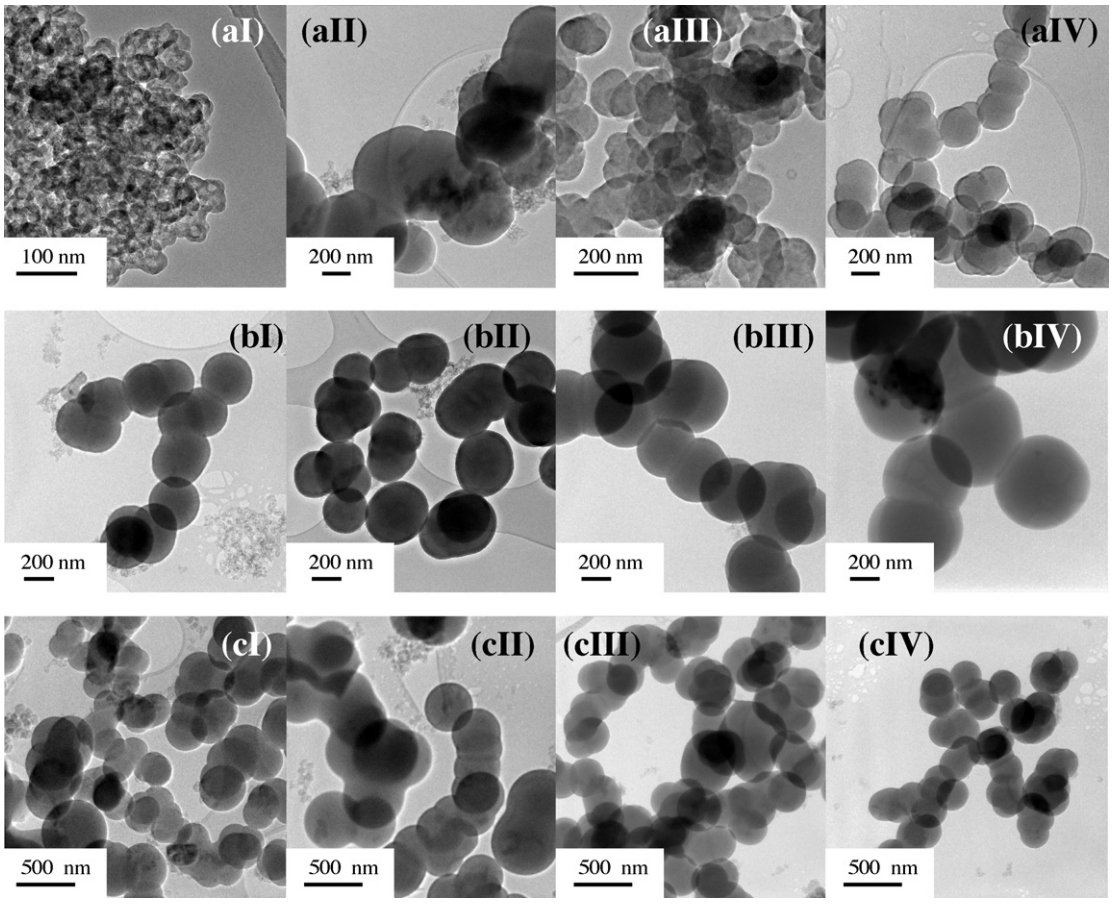


**Fig. 2.** Representative TEM micrographs of the carbon obtained from the pyrolysis of (a) benzene, (b) aniline and (c) nitrobenzene after (I) 15, (II) 30, (III) 60 and (IV) 120 min-on-stream.

in acetone with a drop of the resultant suspension evaporated onto a holey carbon supported grid. CNS size distributions presented in this report are based on particle counts in excess of 400. Temperature-programmed oxidation (TPO) profiles of the carbon product were obtained using a Perkin-Elmer TGA7 thermogravimetric analyzer where a 10 mg sample was ramped from room temperature to 1000 °C at 5 °C $min^{-1}$ in a 50 $cm^3$ $min^{-1}$ $O_2$/He (20%, v/v). The carbon, hydrogen and nitrogen (CHN) content in the solid carbon deposits was determined using a LECO CHNS-932 apparatus. The carbon (*ca.* 2 mg) combustion (at 950 °C) products were analysed by IR (for C and H content) and thermal conductivity detector (TCD) (for N content). XPS analyses were performed in a SPEC Phoibos system operating with Al (Kα) radiation. Peak areas were determined using Shirley's method and the spectra were fitted with Gaussian curves. Sensitivity factors for peaks C1s and N1s were 1 and 1.8 respectively.

## 3. Results and discussion

Carbon yields (grams of solid carbon obtained per gram of carbon in the feed) associated to each hydrocarbon are presented in Fig. 1. An apparent induction period was observed at the first minutes of the synthesis, to approach a uniform solid carbon production after *ca.* 30 min-on-stream. Regarding the nature of the feed, the carbon yields obtained followed the sequence: nitrobenzene < benzene < aniline. Formation enthalpies found in the literature for benzene, aniline and nitrobenzene are 82.6, 87.1 and 67.5 kJ/mol respectively [21], putting in evidence the activating effect of the $-NH_2$ group and the deactivating effect of the $-NO_2$ group respect to the benzene ring and therefore, the relative reactivity of these molecules.

TEM micrographs presented in Fig. 2 show the temporal evolution of carbon synthesized by pyrolysis of benzene, aniline and nitrobenzene. After 15 min-on-stream, benzene conducted to a porous carbon (PC) structure without a defined shape but an ordered arrangement of the graphene layers (Fig. 3a). This structure evoluted to a spherical morphology after 30 min-on-stream, where the spheres did not remain as discrete entities, but rather as a clustering, where some PC was still present. Spheres also exhibited a graphitic structure, as shown in Fig. 3b. This temporal evolution has been reported elsewhere as the consequence of unstable pentagons, hexagons, heptagons or reactive dangling bonds that evolve through bond switching and migration processes to form more stable spherical structures [22,23]. Extended reaction times resulted in the same formation of spheres with subsequent decrease in PC presence. The use of nitrogen containing precursors, such as aniline and nitrobenzene, resulted in the formation of spheres from the first stages of the synthesis. This enhanced curvature of the graphitic sheets in comparison to the carbon product obtained from benzene has been attributed in the literature to a nitrogen-induced reduction of the energy barrier to form pentagons that buckle the graphitic layers, favouring the sphere formation when nitrogen is incorporated in the graphitic matrix [24]. Traces of PC were present in samples obtained at short reaction times, decreasing, as in the case of benzene, at extended reaction times. Results presented above reveal how both time-on-stream and the presence of nitrogen favour the curvature of the graphitic sheets that conduct to the final spherical shape. The final diameter of the CNS obtained (Table 1) did not seem to be sensitive to pyrolysis time nor to the nature of the feed.

BET surface area and pore geometry values associated to all the samples prepared are quoted in Table 1, while representative $N_2$ adsorption/desorption isotherm and pore size distribution are presented in Fig. 4. All the samples presented a type IV $N_2$ adsorption/desorption isotherm with hysteresis loop due to capillary condensation, representative of a mesoporous material. Indeed, the mean pore diameter falls in all the cases within the accepted mesoporous (2–50 nm) range. The low $N_2$ volume adsorbed at low pressures is representative of the low surface area and negligible porosity values recorded and consistent with those reported in the literature [17]. Low surface area associated to CNS is a direct consequence of their spherical morphology, i.e. the sphere is the geometrical body with the lowest exposed surface area. The representative pore size distribution shown in Fig. 4b exhibited a peak maximum at *ca.* 6.3 nm with low associated pore volume, linked to the open edges created by the unclosed graphitic flakes, reported in the literature as surface microstructures [10], and followed by an increase in pore volumes at higher pore diameters. Since no internal porosity has been reported for these materials [25], we tentatively attribute the associated pore volume to the external porosity created by the empty room left by the randomly oriented spherical bodies in the bulk, as illustrated by the TEM pictures presented in Fig. 2. Independently of the hydrocarbon employed as carbon/nitrogen–carbon source, both BET surface area and pore volume decreased when increasing time-on-stream, result that is

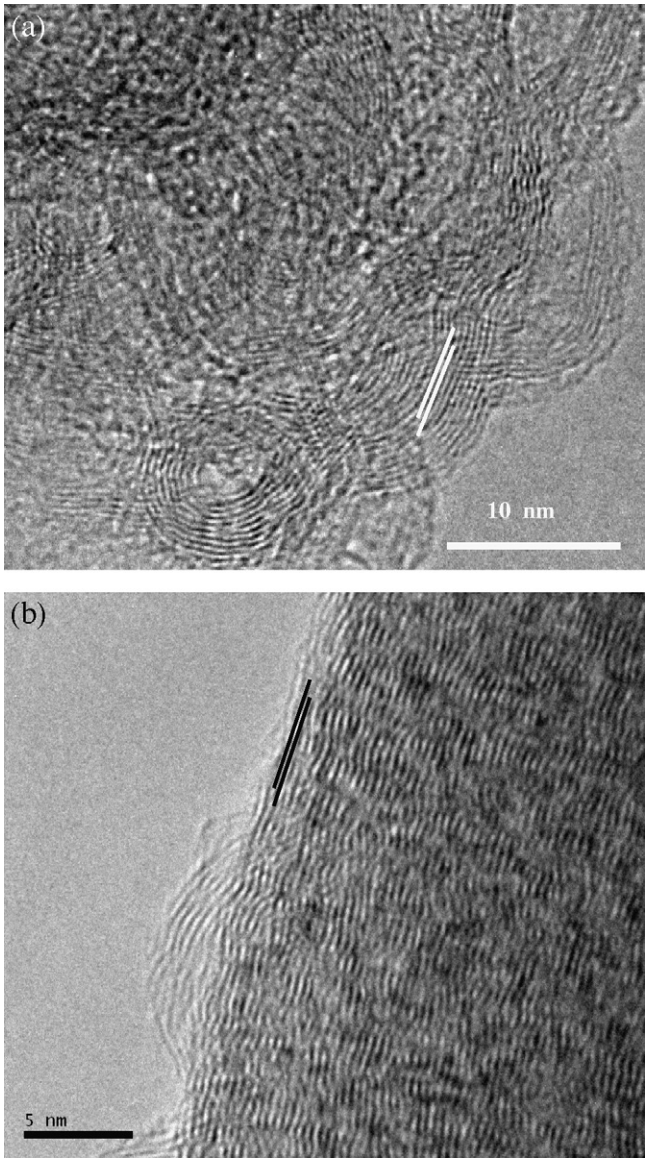


**Fig. 3.** HRTEM micrographs of the carbon obtained from the pyrolysis of benzene after (a) 15 and (b) 30 min-on-stream.

**Table 1**
BET surface area, porosity, crystalline parameters, maximum gasification temperature, elemental (CHN) composition and CNS diameter range.

| Feed | Time-on-stream (min) | BET surface area ($m^2\ g^{-1}$) | Pore volume ($cm^3\ g^{-1}$) | Pore diameter (nm) | $d_{002}$ (Å) | $L_c$ (Å) | $TPO_{Max}$ (°C) | C (mol%) | H (mol%) | N (mol%) | Diameter range (average) (nm) |
|---|---|---|---|---|---|---|---|---|---|---|---|
| Benzene | 15 | 109.5 | 0.31 | 11.5 | 3.37 | 49.5 | 598 | 89.5 | 10.5 | 0 | – |
| | 30 | 66.4 | 0.18 | 15.6 | 3.37 | 100.0 | 607 | 92.6 | 7.4 | 0 | 250–610 (397) |
| | 60 | 25.1 | 0.08 | 12.9 | 3.36 | 56.4 | 610 | 92.8 | 7.2 | 0 | 250–620 (380) |
| | 120 | 14.3 | 0.05 | 13.8 | 3.36 | 33.0 | 625 | 94.2 | 5.8 | 0 | 150–670 (370) |
| Aniline | 15 | 51.5 | 0.16 | 12.5 | 3.37 | 19.3 | 568 | 86.0 | 11.5 | 2.5 | 100–630 (378) |
| | 30 | 31.3 | 0.10 | 12.6 | 3.37 | 32.6 | 586 | 90.7 | 6.2 | 3.1 | 200–640 (361) |
| | 60 | 22.9 | 0.08 | 13.2 | 3.37 | 23.2 | 607 | 92.0 | 4.8 | 3.2 | 200–640 (374) |
| | 120 | 11.8 | 0.03 | 10.9 | 3.36 | 21.9 | 608 | 92.1 | 4.5 | 3.4 | 200–760 (382) |
| Nitrobenzene | 15 | 13.4 | 0.05 | 12.9 | 3.39 | 12.3 | 561 | 81.9 | 15.9 | 2.1 | 200–760 (344) |
| | 30 | 11.4 | 0.04 | 17.6 | 3.37 | 28.3 | 571 | 85.5 | 12.4 | 2.1 | 200–860 (324) |
| | 60 | 9.6 | 0.04 | 16.1 | 3.37 | 19.8 | 592 | 88.6 | 9.0 | 2.3 | 200–1000 (408) |
| | 120 | 9.1 | 0.03 | 15.4 | 3.37 | 18.9 | 604 | 90.4 | 7.0 | 2.5 | 200–760 (330) |

in good agreement with the exposed above, where PC, responsible of higher porosity values, was essentially present at short reaction times. This finding was further accused in the case of benzene, where the PC, as sole reaction product after 15 min-on-stream, delivered a two-fold BET surface area and pore volume than the carbon obtained after 30 min, when the spherical morphology started to be predominant in the bulk. Regarding the nature of the feed, higher surface areas and pore volumes were obtained for the carbon synthesized from benzene. This result is tentatively linked to the absence/presence of nitrogen in the carbon matrix (Table 1), i.e. nitrogen facilitates the curvature of the graphene layers, as commented above, disfavouring the presence of PC and therefore, promoting the formation of spheres, in line with the lower porosity values recorded for the carbon obtained from aniline and nitrobenzene decomposition, essentially remarkable at short reaction times. This morphological change was further investigated by temperature-programmed oxidation analyses (Fig. 5), where the maximum oxidation temperature was consistently shifted to higher values for the carbon obtained at longer reaction times (Table 1), suggesting a better graphitization of the carbonaceous material when adopting the spherical morphology. Lower maximum oxidation temperatures (Table 1, Fig. 5) recorded for carbon obtained from nitrogen containing compounds cannot be explained in terms of carbon overall morphology (PC, spheres) but rather as a consequence of nitrogen inclusion in the material. It is well established that the incorporation of heteroatoms into structured carbon, even at a low mass/mole percent, can induce lattice defects in the graphene layers [26], conducting to a less graphitic material and thus, easier to oxidise. While TPO analysis provides an indirect assessment of carbon structural order, the inferred trends find further support in XRD analyses (see Table 1). Representative XRD patterns are shown in Fig. 6. Each profile exhibits a main peak at *ca.* 25°, i.e. (0 0 2) graphite plane, as well as two secondary

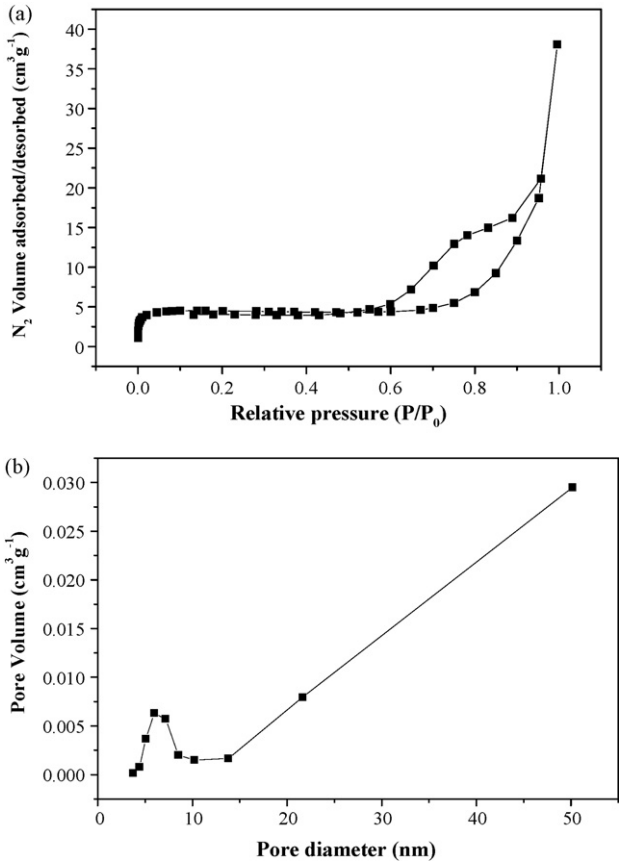


**Fig. 4.** (a) $N_2$ adsorption/desorption isotherm and (b) and pore size distribution associated with carbon obtained from the pyrolysis of benzene after 120 min-on-stream.

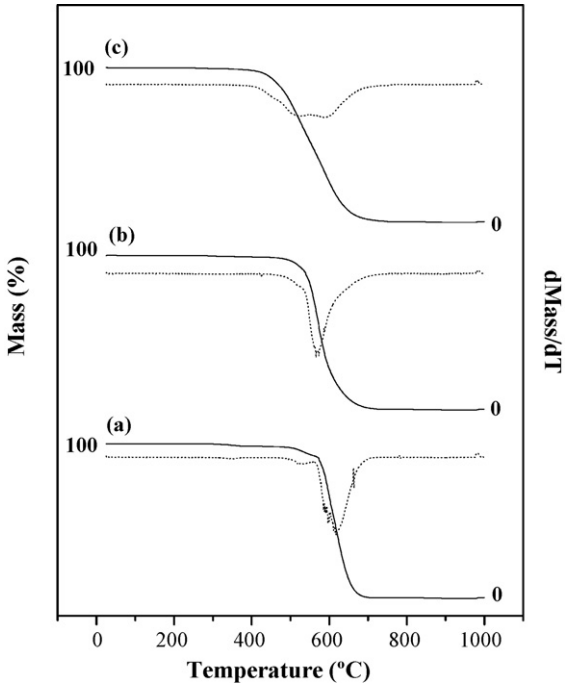


**Fig. 5.** TPO (solid line) and DTG (dotted line) profiles associated with the carbon obtained from the pyrolysis of (a) benzene, (b) aniline and (c) nitrobenzene after 60 min-on-stream.

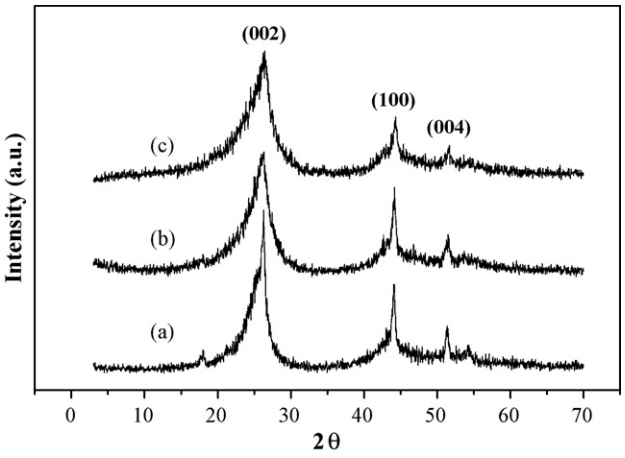


**Fig. 6.** XRD patterns associated with the carbon obtained from the pyrolysis of (a) benzene, (b) aniline and (c) nitrobenzene after 60 min-on-stream.

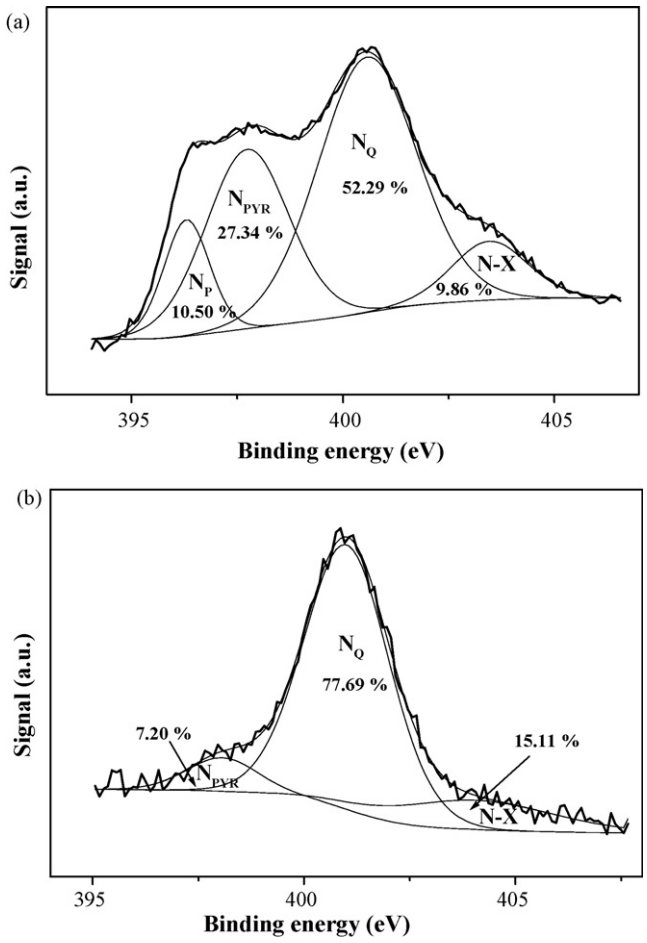


**Fig. 7.** XPS N1s spectrum of the carbon obtained from the pyrolysis of (a) aniline (N = 3.4 mol%) and (b) nitrobenzene (N = 1.0 mol%) after 120 min-on-stream.

reflections at *ca.* 44° and 51.4°, corresponding to (1 0 0) and (0 0 4) graphite planes respectively. We have adopted the interlayer spacing ($d_{002}$, 0.335 nm for graphite) as a quantitative measurement of the graphitic character. The $d_{002}$ values recorded in Table 1 are consistent with a graphitic product where a slight decrease in the interlayer spacing with increasing reaction time suggests a better packing of the graphene layers, which is in good agreement with the results derived from TPO analyses. The average crystalline size $L_c$ (deduced from the half-width of the (0 0 2) diffraction peak) was analysed, presenting a common pattern for the three hydrocarbons employed; $L_c$ increased when synthesis time approached 30 min and decreased at longer reaction times. The initial increase matches the most accused morphogical change (essentially in the case of benzene), when the ill-defined PC evolutes to CNS, being the average crystalline size favoured in the latest structure. Once the PC is negligible in the bulk, the average crystalline size might undergo disruption as the spherical morphology gains definition, where the curved domains play counter a large scale piling up of the graphene layers. Moreover, $L_c$ was always greater in those samples obtained from benzene, confirming how the presence of nitrogen in the carbon matrix induces the presence of lattice defects.

Elemental analysis is shown in Table 1, where nitrogen incorporation was in the range 2.1–3.5 mol%, experiencing a slight increase when increasing reaction time and, as commented above, favouring the formation of the spheres. Nitrobenzene conducted to lower nitrogen incorporation than aniline, in line with its lower reactivity. Elemental analyses also supported the finding that extended reaction times favoured the graphitic character, where carbon content increased when increasing reaction time (with subsequent decrease in hydrogen content), attributable to a more ordered structure, in agreement with the reported in previous studies [27]. CHN elemental analyses provide a measurement of the bulk composition of the material. Therefore, to gain a better understanding of the way in which nitrogen is incorporated into the carbon structures, XPS analyses were performed to selected samples obtained from the pyrolysis of the three hydrocarbons at a fixed reaction time, i.e. 120 min-on-stream. As expected, carbon obtained from benzene did not produce any measurable nitrogen-associated signal, what discards the contribution of physisorbed nitrogen during sample handling/preparation/analysis. N1s XPS spectra associated to the carbon obtained from the pyrolysis of aniline and nitrobenzene are presented in Fig. 7. After deconvolution of the N1s peaks, at least three different signals were fitted, revealing the presence of different nitrogen functionalities. Nitrogen incorporation has been studied in different carbonaceous materials, such as carbon chars [28], carbon nanotubes [29,30] or polymeric carbon [31]. Type and distribution of nitrogen functionalities is strongly dependent on preparation temperature [28,30] or nitrogen–carbon source [30]. Thermal treatment at temperatures of *ca.* 600 °C in the presence of phosphoric acid has also resulted in a modification of nitrogen functionality distribution [31]. The general consensus in literature related to nitrogen-doped carbon assigns nitrogen functionalities to pyridinic nitrogen ($N_P$, BE at *ca.* 398 eV), pyrolic nitrogen ($N_{PYR}$, BE at *ca.* 399 eV), quaternary nitrogen ($N_Q$, BE at *ca.* 401 eV) and adsorbed nitrogen or nitrogen oxides (N–X, BE at *ca.* 402–405 eV). N1s peak associated to carbon obtained from the pyrolysis of aniline (Fig. 7a) exhibited these four contributions, with relative nitrogen amounts of 10.50%, 27.34%, 52.29% and 9.86% corresponding to $N_P$, $N_{PYR}$, $N_Q$ and N–X respectively. In the case of nitrobenzene as nitrogen–carbon source, the best fitting of the N1s peak (Fig. 7b) conducted to three curves, corresponding to $N_{PYR}$, $N_Q$ and N–X, with relative nitrogen amounts of 7.20%, 77.69% and 15.11% respectively, with no appreciable contribution from pyridinic nitrogen. This result suggests a more homogeneous distribution of nitrogen species in carbon obtained from the pyrolysis of nitrobenzene. Quaternary nitrogen, reported in the literature as the most stable functionality at temperatures greater than 600 °C [28,30], was predominant in both cases. Elemental composition obtained by XPS (surface technique, not able to identify hydrogen), cannot be directly compared with the obtained from CHN elemental analysis. However, XPS derived nitrogen content (see caption in Fig. 7) is in quite good agreement with the obtained from CHN elemental analysis, confirming the trend associated to the nature of the

feed, i.e. aniline conducted to a higher nitrogen inclusion than nitrobenzene.

## 4. Conclusions

In the present study, thermal decomposition of benzene, aniline and nitrobenzene has been successfully employed in the controlled growth of CNS, where decomposition time and nature of the feed strongly influenced the nature of the solid product obtained. An increase in decomposition time resulted in enhanced product cristallynity, where the presence of a graphitic but ill-defined carbonaceous deposit (PC) evoluted to a predominantly spherical product (CNS), due to unstable pentagons, hexagons, heptagons or reactive dangling bonds that evolve through bond switching and migration processes to form more stable spherical structures. The presence of nitrogen in the feed resulted in enhanced curvature of the product due to a nitrogen-induced reduction of the energy barrier to form pentagons that buckle the graphitic layers, favouring the sphere formation. Moreover, the incorporation of nitrogen into the carbon matrix, inducing lattice defects in the graphene layers, conducted to a less graphitic material than the obtained in the absence of nitrogen. Nitrogen incorporation was favoured at extended reaction times, as well as for the more reactive aniline. XPS analyses revealed a more homogeneous distribution of nitrogen functionalities in the CNS obtained from nitrobenzene, being the quaternary nitrogen predominant in both cases.

## Acknowledgments

The authors acknowledge financial support from Consejería de Ciencia y Tecnología de la Junta de Comunidades de Castilla-La Mancha (Project PBI-05-038 and PCI08-0020-1239). Dr. Manuel Mora (University of Córdoba) is gratefully acknowledged for assistance in XPS measurements and stimulating discussions.

## References

[1] Y. Fan, B. Liao, M. Liu, Y. Yei, M. Lu, H. Cheng, Hydrogen uptake in vapor-grown carbon nanofibers, Carbon 37 (1999) 1649–1652.
[2] C.N.R. Rao, Novel materials, materials design and synthetic strategies: recent advances and new directions, J. Mater. Chem. 9 (1999) 1–14.
[3] H. Markus, A.J. Plomp, T. Sandberg, V. Nieminen, J.H. Bitter, D.Y. Murzin, Dehydrogenation of hydroxymatairenisol to oxomatairenisol over carbon nanofibre-supported palladium catalysts, J. Mol. Catal. A: Chem. 274 (2007) 42–49.
[4] M. Glerup, J. Steinmetz, D. Samaille, O. Stéphan, S. Enouz, A. Loiseau, S. Roth, P. Bernier, Synthesis of N-doped SWNT using the arc-discharge procedure, Chem. Phys. Lett. 387 (2004) 193–197.
[5] Y. Zhang, H. Gu, K. Suenaga, S. Iijima, Heterogeneous growth of B–C–N nanotubes by laser ablation, Chem. Phys. Lett. 279 (1997) 264–269.
[6] K.P. de Jong, J.W. Geus, Carbon nanofibers: catalytic synthesis and applications, Catal. Rev.-Sci. Eng. 42 (2000) 481–510.
[7] O. Stephan, P.M. Ajayan, C. Colliex, Ph. Redlich, J.M. Lambert, P. Bernier, P. Lefin, Doping graphitic and carbon nanotube structures with boron and nitrogen, Science 266 (1994) 1683–1685.
[8] M. Glerup, M. Castignoles, M. Holzinger, G. Hug, A. Loiseau, P. Bernier, Synthesis of highly nitrogen-doped multi-walled carbon nanotubes, Chem. Commun. (2003) 2542–2543.
[9] T. Maiyalagan, B. Viswanathan, Template synthesis and characterization of well-aligned nitrogen containing carbon nanotubes, Mater. Chem. Phys. 93 (2005) 291–295.
[10] Z.C. Kang, Z.L. Wang, Chemical activities of graphitic carbon spheres, J. Mol. Catal. A: Chem. 118 (1997) 215–222.
[11] P. Serp, R. Feurer, Y. Kihn, J.L. Faria, J.L. Figueiredo, Novel carbon supported material: highly dispersed platinum particles on carbon nanospheres, J. Mater. Chem. (2001) 1980–1981.
[12] W. Qian, L. Wei, F. Cao, Q. Chen, W. Qian, Low temperature synthesis of carbon nanospheres by reducing supercritical carbon dioxide with bimetallic lithium and potassium, Carbon 44 (2006) 1303–1307.
[13] J.-M. Du, D.-J. Kang, Synthesis of carbon nanostructures with unique morphologies via a reduction-catalysis reaction route, Mater. Res. Bull. 41 (2006) 1785–1790.
[14] Z.L. Wang, K.C. Kang, Graphitic structure and surface chemical activity of nanosize carbon spheres, Carbon 35 (1997) 419–426.
[15] Z.L. Wang, K.C. Kang, Pairing of pentagonal and heptagonal carbon rings in the growth of nanosize carbon spheres synthesized by a mixed-valent oxide-catalytic carbonization process, J. Phys. Chem. 100 (1996) 17725–17731.
[16] A. Nieto-Márquez, J.L. Valverde, M.A. Keane, Catalytic growth of structured carbon from chloro-hydrocarbons, Appl. Catal. A: Gen. 332 (2007) 237–246.
[17] A. Nieto-Márquez, J.L. Valverde, M.A. Keane, Selective low temperature synthesis of carbon nanospheres via the catalytic decomposition of trichloroethylene, Appl. Catal. A: Gen. 352 (2009) 159–170.
[18] H.-S. Qian, F.-M. Han, B. Zhang, Y.-C. Guo, J. Yue, B.-X. Peng, Non-catalytic CVD preparation of carbon spheres with a specific size, Carbon 42 (2004) 761–766.
[19] Y.Z. Jin, C. Gao, W.K. Hsu, Y. Zhu, A. Huczko, M. Bystrzejewski, M. Roe, C.Y. Lee, S. Acquah, H. Kroto, D.R.M. Walton, Large-scale synthesis and characterization of carbon spheres prepared by direct pyrolysis of hydrocarbons, Carbon 43 (2005) 1944–1953.
[20] L.C. Yang, Y. Shi, Q.S. Gao, B. Wang, Y.P. Wu, Y. Tang, The production of carbon nanospheres by the pyrolysis of polyacrylonitrile, Carbon 46 (2008) 1816–1818.
[21] O.V. Dorofeeva, N.F. Moiseeva, Standard thermodynamic properties of nitrobenzene in the ideal gas state, Russ. J. Phys. Chem. A 82 (2008) 136–137.
[22] J.Y. Miao, D.W. Hwang, C.C. Chang, S.H. Lin, K.V. Narasimhulu, L.P. Hwang, Uniform carbon spheres of high purity prepared on kaolin by CCVD, Diamond Rel. Mater. 12 (2003) 1368–1372.
[23] Z.X. Xu, J.D. Lin, V.A.L. Roy, Y. Ou, D.W. Liao, Catalytic synthesis of carbon nanotubes and carbon spheres using Kaolin supported catalyst, Mater. Sci. Eng. B 123 (2005) 102–106.
[24] J. Mandumpal, S. Gemming, G. Seifert, Curvature effects of nitrogen on graphitic sheets: structures and energetics, Chem. Phys. Lett. 447 (2007) 115–120.
[25] P. Serp, R. Feurer, P. Kalck, Y. Kihn, J.L. Faria, J.L. Figueiredo, A chemical vapour deposition process for the production of carbon nanospheres, Carbon 39 (2001) 621–626.
[26] A.G. Kudashov, A.V. Okotrub, L.G. Bulusheva, I.P. Asanov, Y.V. Shubin, N.F. Yudanov, L.I. Yudanova, V.S. Danilovich, O.G. Abrosinov, Influence of Ni–Co catalyst composition on nitrogen content in carbon nanotubes, J. Phys. Chem. B 108 (2004) 9048–9053.
[27] T. Renouard, L. Gherghel, M. Wachtler, F. Bonino, B. Scrosati, R. Nuffer, C. Mathis, K. Müllen, Pyrolysis of hexa(phenyl)benzene derivatives: a molecular approach toward carbonaceous materials for Li-ion storage, J. Power Sources 139 (2005) 242–249.
[28] J.R. Pels, F. Kapteijn, J.A. Moulijn, Q. Zhu, K.M. Thomas, Evolution of nitrogen functionalities in carbonaceous materials during pyrolysis, Carbon 33 (1995) 1641–1653.
[29] J. Amadou, K. Chizari, M. Houllé, I. Janowska, O. Ersen, D. Bégin, C. Pham-Huu, N-doped carbon nanotubes for liquid-phase C=C bond hydrogenation, Catal. Today (2008) 62–68.
[30] S. van Dommele, A. Romero-Izquirdo, R. Brydson, K.P. de Jong, J.H. Bitter, Tuning nitrogen functionalities in catalytically grown nitrogen-containing carbon nanotubes, Carbon 46 (2008) 138–148.
[31] Y. Wu, S. Fang, Y. Jiang, Carbon anodes for a lithium secondary battery based on polyacrylonitrile, J. Power Sources 75 (1998) 201–206.